Experimental Testing of Advanced Generalized Predictive Control for Stability Augmentation and Vibration Reduction of Tiltrotor Aircraft

Thomas G. Ivanco
Flight Dynamics Branch
National Aeronautics and Space Administration
Hampton, VA, USA

Andrew R. Kreshock
U.S. Army DEVCOM
U.S. Army Research Laboratory
Hampton, VA, USA

Robert P. Thornburgh
U.S. Army DEVCOM
U.S. Army Research Laboratory
Hampton, VA, USA

Matthew L. Wilbur
Retired, U.S. Army DEVCOM
U.S. Army Research Lab
Hampton, VA, USA

Brett A. Newman
Department of Mechanical and Aerospace Engineering
Old Dominion University
Norfolk, VA, USA

ABSTRACT

Generalized Predictive Control (GPC) is an advanced form of an adaptive control algorithm that uses experimentally acquired data to determine the input-output relationship of complex systems through a process called system identification (system ID). GPC has historically been applied to wind tunnel tests of dynamically-scaled tiltrotor aircraft for stability augmentation and vibration reduction since the complex nature of these dynamic systems does not lend itself well to traditional control theory. Advanced GPC (AGPC) improves upon traditional GPC by enabling self-adaptation as conditions change from those used to acquire the system ID and controller performance would normally erode. The present research expands upon previous analytical development and demonstration of AGPC with experimental demonstration. To support AGPC, this present work also identifies and describes figures of merit that define a good working controller and quantifies the uniqueness of the control inputs and quality of the system ID parameters. The present research demonstrates that AGPC consistently performs better than traditional GPC and can successfully adapt to changing conditions.

NOTATION

AGPC	=	advanced generalized predictive control
ARX	=	autoregressive moving average model with exogenous input
GPC	=	generalized predictive control
h_c	=	control horizon
h_p	=	prediction horizon
k	=	time step index parameter
LVDT	=	linear variable displacement transducer
m	=	number of response measurements (outputs)
OMP	=	Observer Markov Parameters
p	=	order of the ARX equation, number of past inputs and responses in model
Q	=	weighting matrix for control (penalizes control)
r	=	number of control inputs
R	=	weighting matrix for error (penalizes error)
s	=	number of time steps used in system identification
TDT	=	Transonic Dynamics Tunnel, NASA Langley Research Center
TRAST	=	TiltRotor Aeroelastic Stability Testbed
u	=	control input
y	=	response output
ε	=	error between target and measured response (equal to the response for a regulator)
ξ	=	system modeling error between predicted and actual system response (error in OMP)

INTRODUCTION

Tiltrotor aircraft are defining the state-of-the-art in vertical lift technology as they have the potential to greatly expand rotary-wing operational boundaries. However, they are often limited in forward flight speed due to complex coupled rotor and wing dynamic instabilities known as proprotor pylon instability, often referred to as whirl flutter. The U.S. Army and NASA

Presented at the Vertical Flight Society's 79th Annual Forum & Technology Display, West Palm Beach, FL, USA, May 16-18, 2023.

have been developing a new wind-tunnel model, the TiltRotor Aeroelastic Stability Testbed (TRAST), shown in Figure 1, to test proprotors in the NASA Langley Research Center Transonic Dynamics Tunnel (TDT) to investigate these aeroelastic instabilities. The TRAST model is detailed in Ref. 1 and the TDT test capabilities are described in Ref. 2. Part of this investigation includes the use of active controls to stabilize the aircraft beyond the stability boundary and to reduce vibration. Due to the complex nature of tiltrotor aircraft, calculating the dynamic behavior of the aircraft due to control inputs is typically error prone and conventional control methodologies are difficult to employ. Therefore, adaptive control methodologies are typically employed such as generalized predictive control (GPC) which is an advanced form of adaptive control (Refs. 3, 4, and 5). Unique to the current research effort is the development of advanced GPC (AGPC) that offers the ability for the controller to self-adjust as flight or vehicle conditions change. AGPC was first introduced in Ref. 6 and was investigated analytically. This current paper is an extension of that work and investigates the feasibility of GPC and AGPC experimentally, and it introduces figures of merit that were derived to quantify controller performance and reliability. Although the focus of this effort is upon the stabilization of proprotor whirl flutter of a tiltrotor aircraft, the concepts discussed about AGPC and the proposed efforts of this research are applicable to many dynamic systems including fixed wing aircraft. Prior to application of GPC and AGPC to the TRAST model, a simple tiltrotor experimental testbed was developed allowing investigation on an affordable and resilient platform. Following the experimental efforts on the simple tiltrotor model and maturation of the real-time controller interface, GPC and AGPC were tested on the TRAST model in a hover test cell.

This paper will begin with a brief overview of GPC and AGPC. It will then introduce the figures of merit that were developed for AGPC employment. The experimental setup will be presented followed by the experimental results of each testbed. For the experimental results, traditional GPC is presented first then AGPC.

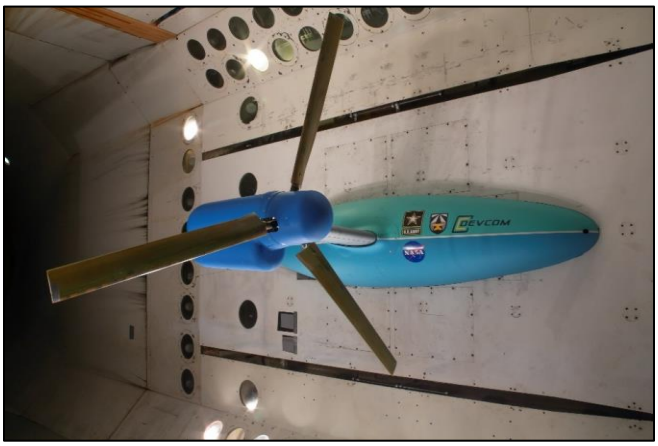

Figure 1. The TiltRotor Aeroelastic Stability Testbed in the Transonic Dynamic Tunnel.

OVERVIEW OF GPC AND AGPC

The concept of GPC was originally introduced by Clarke, Mohtadi, and Tuffs (Ref. 3) as a potential adaptive control algorithm. Reference 3 proposed the concepts of a prediction horizon (h_p), a control horizon (h_c) after which control commands become zero, and a least-squares observer parameter estimator (p), referred to as the order of the model. However, no details are presented in Ref. 3 regarding the parameter computation or system identification. Juang and Phan (Ref. 4) expanded this effort and explored various system identification processes of AutoRegressive moving average model with eXogenous inputs (ARX) models with multiple input multiple output (MIMO) systems and enabled unknown disturbance rejection. Building upon the ARX foundations of Ref. 4 and the GPC introduction of Ref. 3, Kvaternik, Juang and Bennet (Ref. 5) developed an objective function similar to optimal control theory and turned GPC into a practical and powerful MIMO controller. Reference 5 is a foundational, albeit informal, paper describing the state-of-the-art in traditional GPC. Reference 7 explored the use of GPC, as described by Ref. 5, as a tracker for rigid-body control of a flight vehicle.

The derivation of the equations used in the modern traditional GPC controller was presented in Ref. 6 and is further expanded upon in Ref. 8. For clarity, the governing equation is presented here as Equation 1. In this equation, y is the response output, u is the control input, k is the discrete time step index, the prediction horizon (h_p) is the limit of future state estimates, and the control horizon (h_c) is the limit of the finite control horizon after which the controls are assumed to be zero (Ref. 5). Past input and output values are denoted as u_p and y_p respectively and contain p values of u and y. The matrices T, A, and B are described in Refs. 6 and 8 and represent the Observer Markov Parameters (OMP). An experimental system identification (system ID) process, as described in Refs. 6 and 8, is used to determine the OMP matrices. In this paper, "system ID" refers to a successfully computed set of OMP matrices with associated weight values rather than the process of identifying those matrices.

$$y_{h_p}(k) = Tu_{h_c}(k) + Ay_p(k-p) + Bu_p(k-p) \qquad (1)$$

where, the subscripts h_p, h_c, and p denote the size of the respective vectors, and the parenthetical values represent the starting index.

Kvaternik et al. (Ref. 5) present the objective function shown here as Equation 2. Controls u are then determined from minimalization of this function as described in Refs. 5, 6 and 8.

$$J = \varepsilon^T R\varepsilon + {u_{h_c}}^T Q u_{h_c} \qquad (2)$$

where, ε is the error between the target response (y_T) and the predicted response $\varepsilon = y_T - y_{h_p}$, R is the weighting matrix for error, and Q is the weighting matrix for control input.

In the case of a regulator where the target response is zero, the error term ε simply becomes the response *y*.

Traditional GPC is a very effective controller that has been used in many dynamic systems (Refs. 5-9) and often outperforms other control options with regard to successful dynamic suppression and control robustness (Ref. 8). However, the performance of traditional GPC can erode as conditions change from those used to derive the system ID. In aircraft systems, these changes can be a change in flight condition, payload, fuel load, airspeed, or other flight characteristics. Therefore, a drawback of GPC is that it must continually be updated with new system ID acquisitions as conditions change. These new system ID acquisitions introduce disturbances that counter the whole purpose of having a vibration reduction controller. Additionally, some scenarios such as flight beyond a flutter boundary may not allow the acquisition of a new system ID due to the dynamic response of the aircraft and resulting signal to noise ratio.

To enable self-adjustment of a working GPC controller, the concept of AGPC was developed. Reference 6 introduces AGPC and the definition of a system error term (ξ) that can be numerically determined from measured data using Equation 3 after the system described by Equation 1 progresses at least h_p timesteps beyond *k*. The significance of this development is that a working controller can be improved or updated by changes to the OMP matrices done by observation of the input-output relationships during controller operation.

$$\begin{aligned}\xi &= y_{h_{p_{actual}}} - y_{h_{p_{predicted}}} + \{\varphi\} \\ &= y_{h_{p_{actual}}} - \left[T u_{h_{c\,actual}}(k) + A y_p(k-p) + B u_p(k-p)\right] + \{\varphi\}\end{aligned} \tag{3}$$

where φ represents noise and external disturbances.

The subscript *actual* in Equation 3 indicates the actual measurements of response and control inputs after an additional h_p timesteps occur beyond *k*. If one were to assume that the noise and disturbances represented by φ follow a random pattern, then repeated computations should cancel these disturbances. If we continue to an additional *s* timesteps, then one would have *s*-h_p computations of ξ to minimize the effect of φ. If φ is minimized and all the values of *y* and *u* shown in Equation 3 are now measured, then the only uncertainty that should remain is the error (or "delta" values) in the observer matrices *T, A,* and *B*. After these *s* timesteps, Equation 3 can be expanded into the matrix form shown in Equation 4 where the delta operator indicates the error in the observer *T, A,* and *B* matrices where the control and state matrices are of width *s*-h_p. The delta matrix values can then be determined by Equation 5 and the updated values of *T, A,* and *B* by Equation 6.

$$[\xi] = [\Delta T \mid \Delta A \mid \Delta B] \begin{Bmatrix} \left[u_{h_{c\,actual}}\right] \\ \left[y_p(k-p)\right] \\ \left[u_p(k-p)\right] \end{Bmatrix} \tag{4}$$

$$[\Delta T \mid \Delta A \mid \Delta B] = [\xi] pinv\left(\begin{Bmatrix} \left[u_{h_{c\,actual}}\right] \\ \left[y_p(k-p)\right] \\ \left[u_p(k-p)\right] \end{Bmatrix}\right) \tag{5}$$

$$\begin{aligned} T_{new} &= T_{old} + \Delta T \\ A_{new} &= A_{old} + \Delta A \\ B_{new} &= B_{old} + \Delta B \end{aligned} \tag{6}$$

FIGURES OF MERIT FOR AGPC

As previously described, AGPC uses additional data while the controller is operating to compute errors in the system model OMP matrices. With the additional data, the modelling errors can be minimized, and the controller can adapt to changing conditions to build upon an existing "good" system ID.

The challenge of an adaptive controller that self-corrects is that it should only correct the errors of a controller and not worsen a good performing controller. With a good performing controller, there may be little system response or actuator workload, and adaptive metrics may be clouded by signal noise causing very poor adaptive corrections. Therefore, various figures of merit were investigated to quantify the goodness of an operating controller and how reliable adaptive corrections may be.

To quantify the effectiveness of the controller, the magnitude of the objective function was analyzed since the purpose of the controller is to minimize this function. In the absence of other information, a good benchmark for comparison is the magnitude of this objective function during the system ID acquisition assuming that the system was stable and the signal to noise ratio was adequate but not excessive. The objective function equation, recall Equation 2, produces a matrix. An effective scalar equivalent is the largest absolute value from within that matrix. Once an effective controller is implemented, one can then subjectively determine how large the objective function value should be based upon acceptable system behavior. Recall that the objective function is a quantitative value reflecting the magnitude of the system response and controller workload with appropriate weighting matrices *R* and *Q* applied. Therefore, the maximum absolute value of the objective function acquired during a good system ID process is a reliable figure of merit to determine the "goodness" of the controller since the desired weighting is already included.

In addition to the performance or effectiveness of the controller, quantifying the likelihood of the self-adaptive routine to improve performance is important. Proper system

ID requires that the controls be distinguishable from one another. For example, consider simultaneous actuator motion of a tiltrotor swashplate to enable a collective input that suppresses a wing out-of-plane bending vibration when in the helicopter-mode. If the control u consists of individual actuator positions, then all controls are moving in unison. Using these data and associated system ID (or system ID improvement) to determine the relationship to control other modes, such as a wing-chord mode, is not possible. Self-adaptive correction to the matrices in this case could cause erratic behavior in the chord response. Therefore, another important metric is the orthogonality or independence of the various controls to quantify control uniqueness.

Control orthogonality or uniqueness was investigated in two manners. First, the vector product of the three independent commands was computed for the time history. Second, the pairwise correlation coefficient between the various controls (and responses) were computed based upon the relation shown in Equation 7 to determine data collinearity as described by Refs. 9, 10, and 11. For purely orthogonal controls, the vector product determined by the first method should be zero. This was a useful metric in early attempts. If the vector product was orders of magnitude less than the individual signal amplitudes, then the likelihood of a reliable system ID was high. During the physical experiments, this metric was less useful, and it was difficult to determine a meaningful limit to this value. As the controls worked harder, for example, the value of the product increased yet the controls may still have been unique enough to derive a reliable input-output relationship. By contrast, the second method using the correlation coefficient between control channels (Equation 7) was normalized by control magnitude making it more adaptable to different systems or levels of workload. References 9 through 11 specify that a correlation coefficient of less than 0.9 is required to ensure that data collinearity problems do not exist. The system ID efforts in this study using either orthogonal multisines or band-limited white noise with independent seeds resulted in correlation coefficients below 0.1 indicating that the excitation command uniqueness was more than adequate. However, command signals generated from controller employment during closed-loop operation may not meet this uniqueness requirement. Therefore, the correlation coefficients must be monitored before employing AGPC to self-adapt the system ID (Ref. 8). If the correlation coefficients are inadequate, then dither, preferably in the form of orthogonal multisines, must be added to the commands to improve the coefficients. By monitoring these coefficients, the minimal amount of required dither can be determined in order to minimize excitation of the system and maintain favorable response.

$$ru_{ij} = \frac{(u_i - \overline{u_i})^T (u_j - \overline{u_j})}{\sqrt{(u_i - \overline{u_i})^T (u_i - \overline{u_i})}\sqrt{(u_j - \overline{u_j})^T (u_j - \overline{u_j})}} \qquad (7)$$

where the subscripts i and j denote the control number, the bar ($\overline{\ }$) denotes the mean, and $i \neq j$.

In addition to quantifying the performance of the controller and uniqueness of the inputs, two other metrics were employed to quantify the quality of the system ID fit to the system behavior. The first is the coefficient of determination (R^2) for each response and the second is the normalized residuals computed as the residuals normalized by 3σ where σ is the standard deviation of each response time history. Equations for the coefficient of determination are available from multiple sources and is shown here as Equation 8. The residual is simply the difference between the model-predicted response value minus the actual as was shown previously in Equation 3.

Example figures of merit values follow for the system ID acquired for an example five degree-of-freedom (5DOF) linear mass-spring-damper system with response being the velocity of masses 1, 2 and 4 and commands being force applied to masses 1, 3 and 5. The simple 5DOF system is described in detail in Ref. 8 and included simulated measurement noise and unknown external disturbance. Figure 2 shows time history simulation data alongside corresponding predicted values using system ID results. A close-up of a portion of this time history is shown in Figure 3.

$$R^2 = 1 - \frac{RSS\left(y_{hp_{actual}} - y_{hp_{predicted}}\right)}{RSS\left(y_{hp_{actual}}\right)} \qquad (8)$$

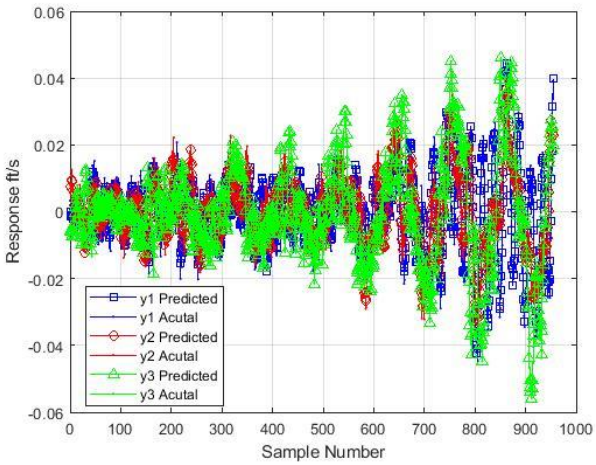

Figure 2 Actual and predicted system response from a 5DOF simulation to develop figures of merit.

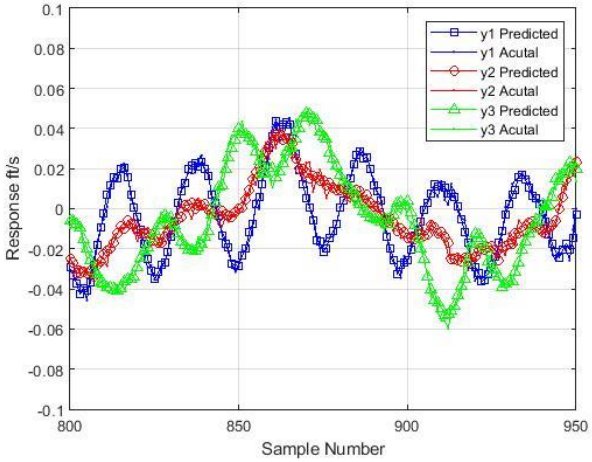

Figure 3. Portion of time history of actual and predicted system response from 5DOF simulation.

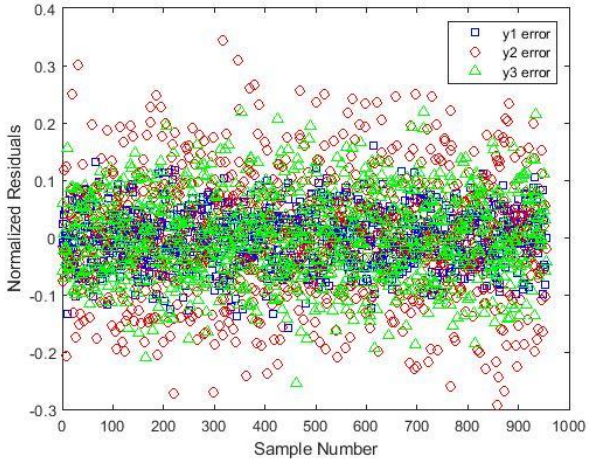

Figure 4. Normalized residuals for Time History of 5DOF Simulation.

For the simulation shown in Figure 2 and Figure 3, the coefficients of determination for *y1*, *y2*, and *y3* are 0.9794, 0.9041, and 0.9492 respectively. These high values of coefficients indicate that the system ID produces a good approximation of the system response behavior. Additionally, the pairwise correlation coefficients between commands 1 and 2, commands 1 and 3, and commands 2 and 3 are 0.0146, 0.0295, and 0.0028 respectively and between the responses 1 and 2, responses 1 and 3, and responses 2 and 3 are 0.6368, 0.6606, and 0.2746 respectively. Therefore, the responses are distinguishable (less than 0.9 per Refs. 9 and 12), and the excitation commands have low correlation and are nearly orthogonal. Additionally, a qualitative assessment can be done by reviewing Figure 2 and Figure 3, where the system ID provides a good model to the system behavior. The lowest coefficient of determination corresponds to the response *y2* where the signal noise magnitude appears relatively higher by comparison to the responses *y1* and *y3*. Normalized residuals (normalized by 3σ) for the time histories are shown in Figure 4. As one can see, the residuals are higher for *y2* and correspond to the lower coefficient of determination for that response.

The behavior of the residuals is favorable. They are scattered about zero indicating that the system ID results do not contain a static offset in system behavior. Additionally, no discernable pattern or trend is recognizable as a function of sample number (or time) indicating that there are no deterministic components remaining and that the system residuals are satisfactory (Ref. 9).

The final figures of merit that were used to quantify the validity of the system ID were the rank and maximum absolute value of the objective function. The rank of the objective function matrix will lend insight into the distinguishability of the response measurements and the independence (degree of orthogonality) of the command inputs. For the system ID acquired above, the objective function produces a matrix of size 954x954 (1000 samples with order p=20, and prediction/control horizon $h_p = h_c = 25$ such that 1000-20-25-1=954). For these results, the rank of the objective function was 150. Since the system ID results are favorable, this value of 150 serves as a guide to determine if the distinguishability of the response and orthogonality of the commands during operational use of the controller at various conditions are adequate to provide reliable identification of the system with the controller active. If the objective function rank is too low, or the orthogonality parameter too high, then dither can be added to the controls to improve the distinguishability when self-adaptive AGPC is attempted. The value of 150 is far removed from the size of the objective function matrix and one may conclude that many rows or columns are linear combinations of other rows or columns. Since the ARX model is an autoregressive model that builds upon previous samples to develop a regressive time history, each time step builds a new row shifted in index from the other rows. With the example sample size, order of the model, and horizon values shown, a rank of 150 is about the highest value that one should expect with these parameters. As model order, sample size, control horizon, or prediction horizon changes, then an acceptable rank value will also change. Therefore, the user needs to develop an understanding of the model to determine acceptable figures of merit.

EXPERIMENTAL SETUP

The real-time controller used for all experimental testing in this paper is the dSPACE® MicroLabBox 1202. MATLAB®

Simulink GPC software was run in dSPACE after conversion to an executable using the "X in the loop" (XIL) standard application protocol interface (API). A signal definition file was also generated as part of the MATLAB conversion and was used to link the dSPACE controller to the software interface called "Control Desk." An additional hurdle with running GPC is the need to run complex matrix computations that are far more convenient to run in MATLAB scripts. Therefore, MATLAB to dSPACE model access port (MA-Port) connections were established that enable the real-time reading and writing of variables to and from MATLAB and dSPACE.

Simple Tiltrotor Model

The miniature simple tiltrotor model was constructed from off-the-shelf miniature radio controlled (RC) helicopter parts and robotic servos. A Blade mCPX BNF was chosen as the helicopter model because it was very small with an eight-inch rotor diameter allowing it to fit inside of a small wind tunnel, and it utilizes a fully articulated swashplate allowing collective and cyclic control. To obtain the required frequency response of the controls, high-performance Park GWS HPX F robotic servos were utilized. These servos are much larger than what is specified for the Blade helicopter, and they also have increased torque and speed enabling adequate frequency response up to 15 Hz. To control the servos, a maestro "Micro 6" 6-channel circuit board was integrated with the servos to convert voltage magnitude from the real-time controller into servo specific pulse-width-modulation (PWM) commands. With this circuit board setup, the real-time controller could output its typical voltage commands as it would do for hydraulic servo actuators. Therefore, the same GPC controller hardware and software was used for the simple tiltrotor model and the more complex TRAST model. Images of the simple tiltrotor model are shown in Figure 5 highlighting the design details and an image of the small wind tunnel is shown in Figure 6.

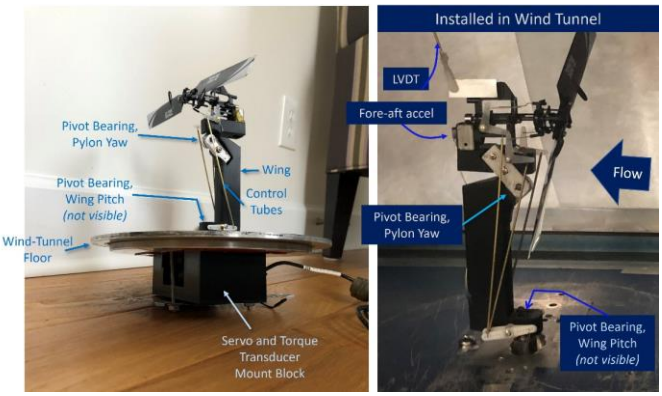

Figure 5. Simple tiltrotor model for small wind tunnel.

Figure 6. Small wind tunnel used for simple tiltrotor model.

To create the dynamic characteristics of a tiltrotor whirl flutter instability, pylon pitch and yaw degrees of freedom must be allowed. These degrees of freedom were achieved with the use of C-Flex pivot bearings to provide lowly-damped hinge axes with acceptable spring rates. C-Flex pivot bearings are barrel shaped and provide linear stiffness with angle. The stiffness is achieved with cruciform beam connections on the interior of the barrel components, and angular displacement is limited by contact between internal barrel structures as the bearing rotates. This limitation in angular displacement by a hard stop of the flexure serves to limit amplitude for any dynamic instability encountered by the wind-tunnel model and allows it to safely go beyond the flutter boundary.

Instrumentation included a torque transducer mounted to the wing base, accelerometers mounted to the nacelle, and a linear variable displacement transducer (LVDT) measuring nacelle motion. Additional details of the simple tiltrotor model and data acquisition are provided in Ref. 8.

TRAST Model

The TRAST model was described in detail in Ref. 1 and described briefly in Refs. 6 and 8. Applying an active control system to a complex rotorcraft model such as TRAST requires an incremental approach due to the risk to the model and facility. A dynamically-scaled rotor system on a flexible model with high-frequency hydraulics has the potential for catastrophic results should the controller fail, even on a hover test stand. Therefore, application of GPC and AGPC to the TRAST model was done first on the model with no blades and no rotation of the rotor system. The only control effector in this configuration was the mass of the swashplate thereby minimizing the risk to model systems. Once the controller and safety protocols proved satisfactory, the rotor system was rotated without the blades installed to verify that motor and drivetrain dynamics and associated electrical loads would not interfere with the controller. Finally, blades were added, and

the model was run in the hover configuration with GPC and AGPC active.

The hover test cell is located in a high-bay area to allow significant air flow through the rotor system. Additionally, the model is surrounded by a safety cage, and it has an additional catch screen in the plane of the rotor system. Due to the orientation of the catch screen, rotor-on operations can only occur in the helicopter mode in the hover test cell. Photos of the TRAST model with an inertial shaker and external shaker are shown in Figure 7. The inertial shaker has an internal mass that vibrates whereas the external shaker is mounted to a stand with a rod directly connecting to the wing spar. Aerodynamic fairings are removed in these images to allow the installation of the inertial shaker and the external shaker attachment rod. With the fairings removed, the natural frequencies of the system increase slightly.

Unlike the simple tiltrotor model, the TRAST model is precision manufactured and contains research-grade instrumentation. Instrumentation includes eight accelerometers (g) located in the engine nacelle, three accelerometers (g) in the wing, three LVDTs measuring swashplate actuator position (in), beam, chord, and torsion bending moment strain gauges (in-lbs) along the wing at three span locations, 9, 23, and 32 inches from the root, diaphragm spring gauges measuring strain (microstrain) at six locations, pitch spring force (lbs), azimuth encoder (deg), and various other rotor and drive train instruments measuring blade position and component loads as described in Ref. 1.

The first out of plane wing bending mode is about 5.1 Hz, the in-plane (chord) bending mode is about 6.8 Hz, and the pylon pitch mode is about 10.4 Hz with fairings installed in the nominal testing configuration. Nominal rotor speeds are 909 rpm in hover and 727 rpm in airplane mode.

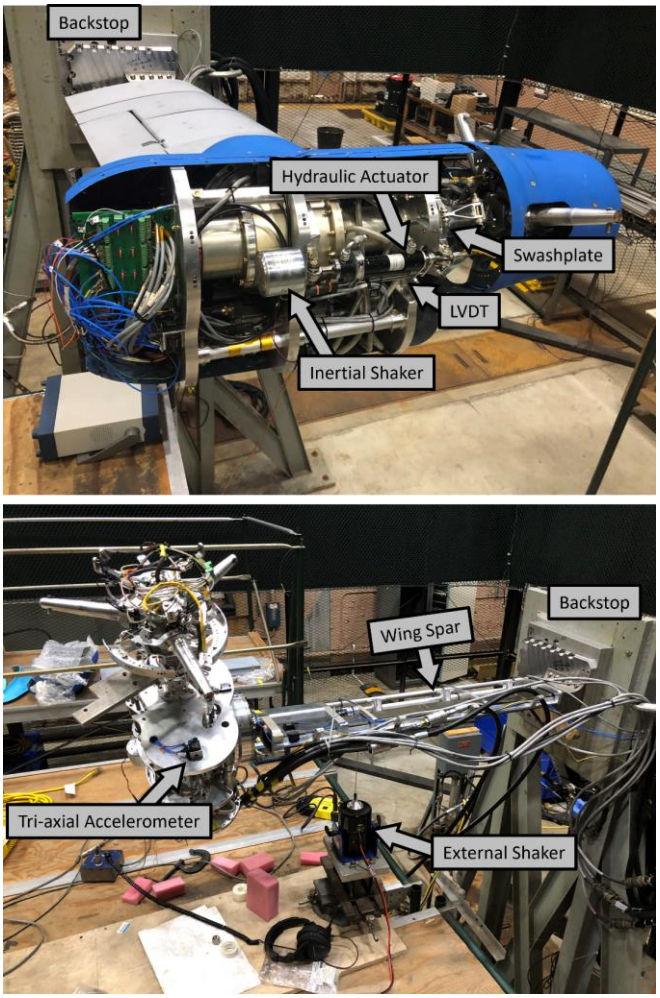

Figure 7. TRAST model details with shakers connected.

EXPERIMENTAL RESULTS

Similar to the analytical investigation presented in Ref. 6, GPC effectiveness and the ability of AGPC to improve controller performance was evaluated experimentally. For comparison, traditional GPC and AGPC performance is presented. Experimental results will first be shown for the simple tiltrotor model and then for the TRAST model.

Traditional GPC Applied to the Simple Tiltrotor Model

Test iterations of the simple tiltrotor model consisted of the following procedure. All cyclic commands were zeroed, and the model swashplate was leveled using servo biases such that it was perpendicular to the rotor shaft. Model controls and operation were then verified. If needed, servo ratio gains were adjusted to maintain a level swashplate at all values of collective pitch. Blade pitch was adjusted to a positive value to encourage windmilling of the rotor system. Model instrumentation was tared to zero load/acceleration values, and the wind tunnel was brought online and slowly increased in velocity. There was no instrumentation available to measure rpm on this small model. Therefore, collective pitch

was adjusted until visual and audible cues for rpm looked and sounded proper at a moderate wind-tunnel speed. Once set to an acceptable value, collective pitch was not adjusted as tunnel velocity was changed or the controller was engaged. The acceptable collective pitch and servo bias/ratio values were noted and were used for subsequent tunnel runs in order to conduct every run at the same nominal collective and cyclic values. As tunnel velocity increased, rotor rpm would also increase. At various velocity values from near idle until an instability was reached, system IDs were acquired, and closed-loop control was verified. At stable tunnel conditions that experienced minimal vibration or motion of the model, the closed-loop controller had almost no effect on the model response other than a slight reduction in vibration. The wind tunnel velocity was increased until an instability was encountered, or model limits were reached indicated by excessive drag deflection of the model. Once an instability was encountered, the tunnel velocity was slowed to a stable condition and a new system ID acquired. Then the adequacy of the closed-loop controller was tested as the model was returned to the unstable velocity. During some runs, attempts were made to acquire a new system ID beyond the flutter boundary, but these were usually unsuccessful as the model response was too large to enable identification of the effects of control inputs.

It was discovered through testing that a good system ID was one that was acquired at a sub-critical velocity (not flutter) with enough excitation to notably move the model but not so much as to cause the rotor disk to stall, diverge, or otherwise change the inflow velocity. Additionally, early GPC attempts resulted in the controller commanding aggressive collective commands to essentially stop the rotor. While this did indeed quell vibration to near-zero values, it is not the intent of the controller. Therefore, a large weighting penalty was applied to collective commands in order to favor cyclic inputs as a solution to vibration reduction. With the larger penalty on collective, the adaptive controller implemented negligible change to collective and rotor rpm.

Shown below in Figure 8 is an example of the open-loop response for an equivalent airspeed of 19.06 ft/s with a nominal collective setting. In this model configuration, the LVDT is attached, a fore-aft accelerometer is installed, and the torque transducer is attached at the model base. Additionally, the control rod linkages are in their nominal configuration to instigate a whirl-flutter instability at low velocity (Ref. 8). The tunnel condition of 19.06 ft/s is just below the whirl-flutter boundary, and some small oscillations are starting to beat in and out during the time history as observed in Figure 8. The response measurements are g's of acceleration for the accelerometer and arbitrary values for the torque transducer and LVDT scaled to have peak responses of similar magnitude. The command signals are voltage of command output. Similarly, shown in Figure 9 is a time history of the system ID excitation and response acquired at a velocity of 19.06 ft/s.

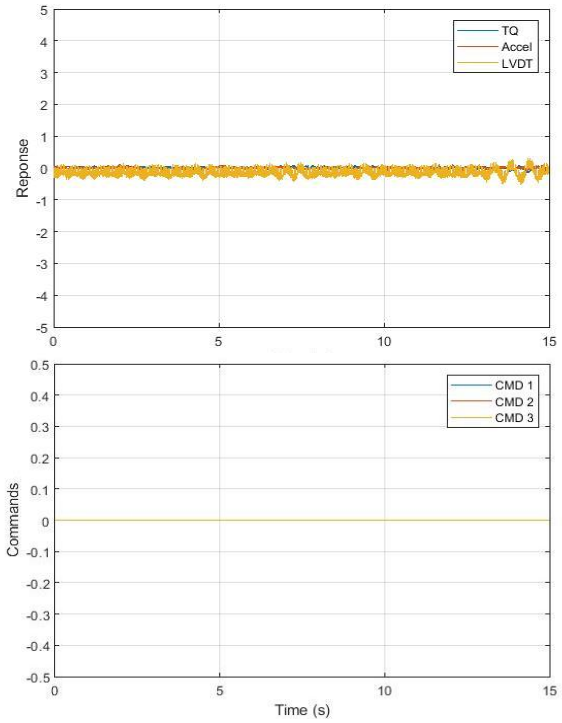

Figure 8. Open-loop response of simple tiltrotor model, V=19.06 ft/s.

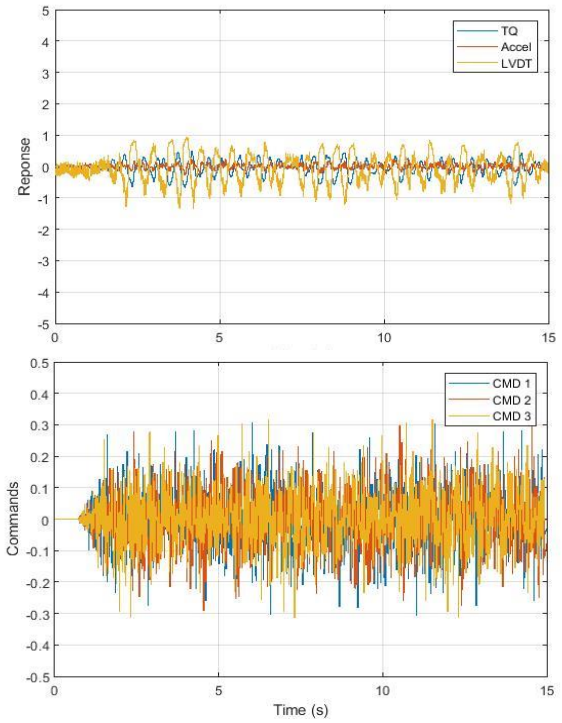

Figure 9. System ID of simple tiltrotor model, V=19.06 ft/s.

The closed-loop response following the system ID is shown in Figure 10. By comparison with Figure 8, one can see that the dynamic response is slightly reduced. The biggest change is the reduction of the low frequency bursting observed near the end of the time history in the open-loop response.

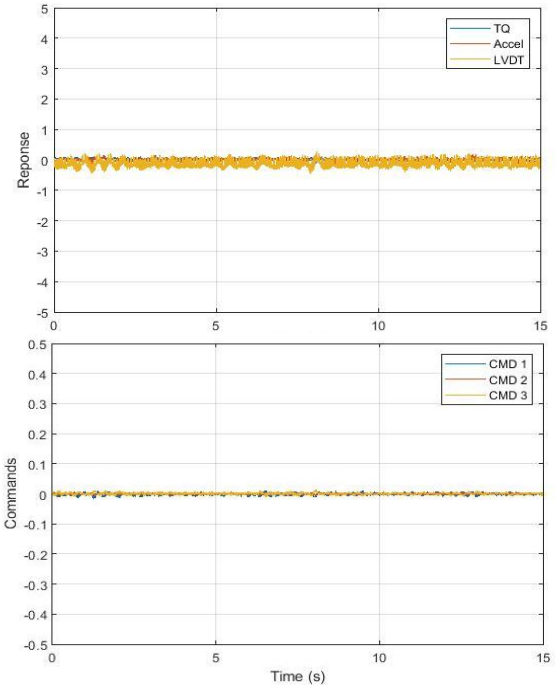

Figure 10. Closed-loop response of simple tiltrotor model, traditional GPC, V=19.06 ft/s.

The effectiveness of the GPC controller is reduced as the model crosses the stability boundary and the system dynamics change considerably. This can be partially explained by difficulty in acquiring a good system ID with the highly non-linear system and challenges associated with the small-scale instrumentation and model quality. For example, the geometry of the yaw LVDT attachment results in highly nonlinear measurement of nacelle yaw that is heavily coupled with wing pitch. Figure 11 shows a time history plot of the closed-loop response of the system in the supercritical flutter condition at 21.17 ft/s with a system ID acquired at 19.06 ft/s. In this figure, the LVDT signal has many repeating spikes showing a periodic yaw-divergence of the system. The controller is struggling to stop this motion, but other dynamics have been suppressed. By comparison, the open-loop response of the model is shown in Figure 12. The command signal is zero for this condition similar to the open-loop response shown in Figure 8, so the plot is not included here. The open-loop response exhibits a large peak-to-peak magnitude of the LVDT measuring nacelle yaw that fluctuates both positive and negative. Additionally, the open-loop response has significant motion of the torque transducer indicating periodic motion of the wing in pitch. This open-loop response resembles a classic whirl-flutter behavior. While the GPC controller is performing poorly, it is able to suppress the whirl motion. Better measurement of the nacelle yaw motion is likely to result in better controller performance.

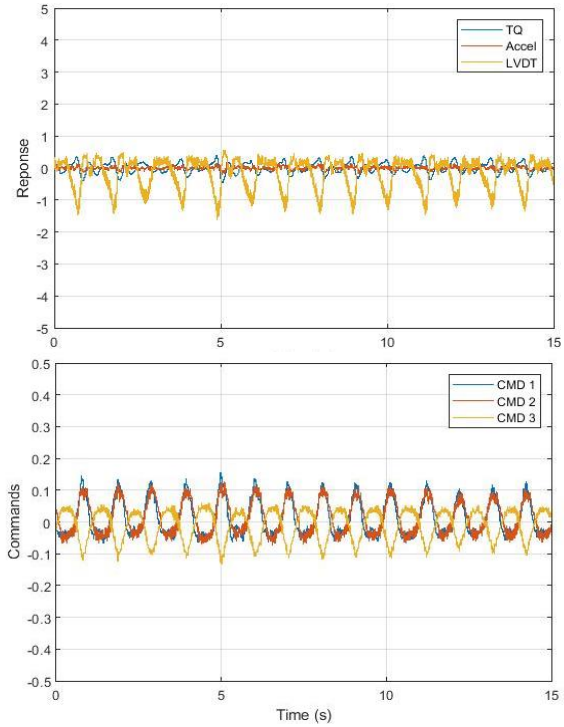

Figure 11. Closed-loop response of simple tiltrotor model, system ID acquired at 19.06, traditional GPC, V=21.17 ft/s.

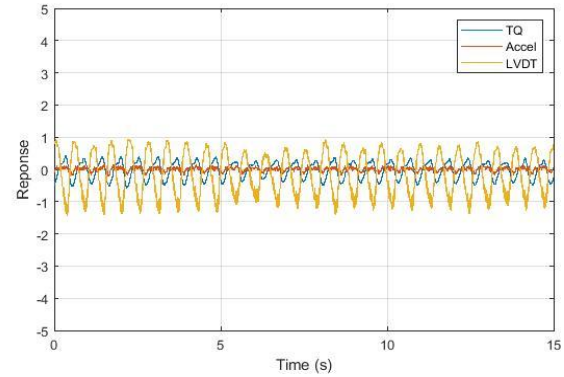

Figure 12. Open-loop response of simple tiltrotor model, V=21.17 ft/s.

To improve controller performance, a new system ID was acquired at 21.17 ft/s with the controller already closed loop with the previous system ID acquired at 19.06 ft/s. The system ID time history is shown in Figure 13, and the closed-loop response of the system with the updated parameters is shown in Figure 14. During this time history, the controller was turned on and off to verify the change in response due to the controller input. As observed, the controller is not able to stabilize the system at this condition. The dynamics of the instability are too overwhelming to allow the signal-to-noise ratio required to acquire a good system ID. Multiple attempts were made, but the controller performance could not be improved at this condition with traditional means.

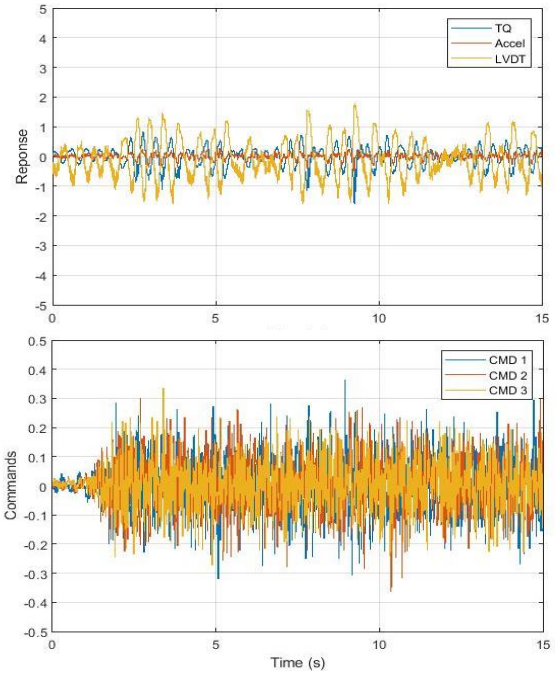

Figure 13. New system ID acquired at V-21.17 ft/s while closed-loop with previous system ID acquired at 19.06 ft/s, attempt to improve traditional GPC.

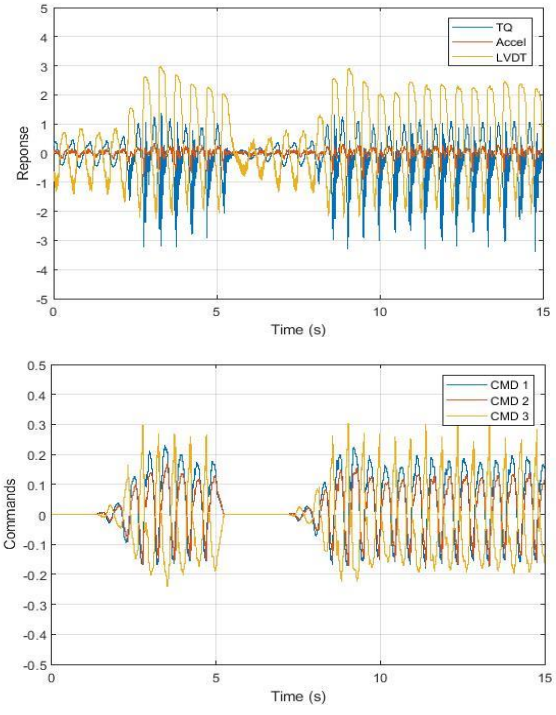

Figure 14. Closed-loop response of simple tiltrotor model with updated system ID, V=21.17 ft/s, traditional GPC with new system ID.

AGPC Applied to the Simple Tiltrotor Model

Similar to the analytical investigation presented in Ref. 6, AGPC was applied experimentally to improve the controller response. AGPC is employed first as a traditional GPC controller while observing the input-output behavior to compute errors in the OMP matrices. For this example, traditional GPC was operating using the system ID previously described and operational in Figure 14. During this employment of AGPC, the figures of merit were not favorable indicating that the commands were not independent enough from one another using the natural closed-loop command and response signals. Therefore, dither was added to the commands until the figures of merit were at adequate levels approaching those achieved during the sub-critical system ID. A time history of the closed-loop controller with dither added is shown in Figure 15 using orthogonal multisine excitation (Ref. 9) added to the natural closed-loop commands. The first part of the time history uses the same system ID matrices as those used for the closed-loop response previously shown in Figure 14. Notice that command excitation is increased, due to the addition of dither, from peak values near approximately 0.3 in Figure 14 to peak values near approximately 0.5 in Figure 15. Despite the addition of the dither, the response magnitude of the system is approximately the same, indicating that the dither has a negligible impact on system response yet significantly improves the figures of merit. The latter part of this time history is with the new controller produced from the AGPC self-correcting algorithm applied, at first with dither still active and finally with the dither stopped. Again, one can observe that the dither has a negligible effect on system response. The advantage of AGPC is apparent in Figure 15 and its performance far outperforms traditional GPC even when the system ID for traditional GPC is attempted at the same condition. In this example, only AGPC could stabilize the system where traditional GPC methods failed despite efforts to acquire new system IDs.

The time history presented in Figure 15 is an example of a favorable self-adaptation attempt where the new OMP matrices are immediately applied to the model as soon as they are calculated by the AGPC algorithm. Other attempts were not as successful during earlier testing, and the control commands quickly became violent. The risks presented to both the simple tiltrotor model and to the wind tunnel used in this experiment were minimal, and experimentation such as this was reasonable. However, as more complex and expensive models and wind tunnels are used, immediate incorporation of newly computed parameters is not wise at the current maturity level of the AGPC technology. Therefore, self-adaptive control changes computed by AGPC were hereafter applied to a controller OMP matrix set that was not in use. Manual mixing of the matrix sets was then done to enable a slow transition from one matrix set to another allowing the investigator to observe the change in system performance before committing to the self-adaptive AGPC controller update.

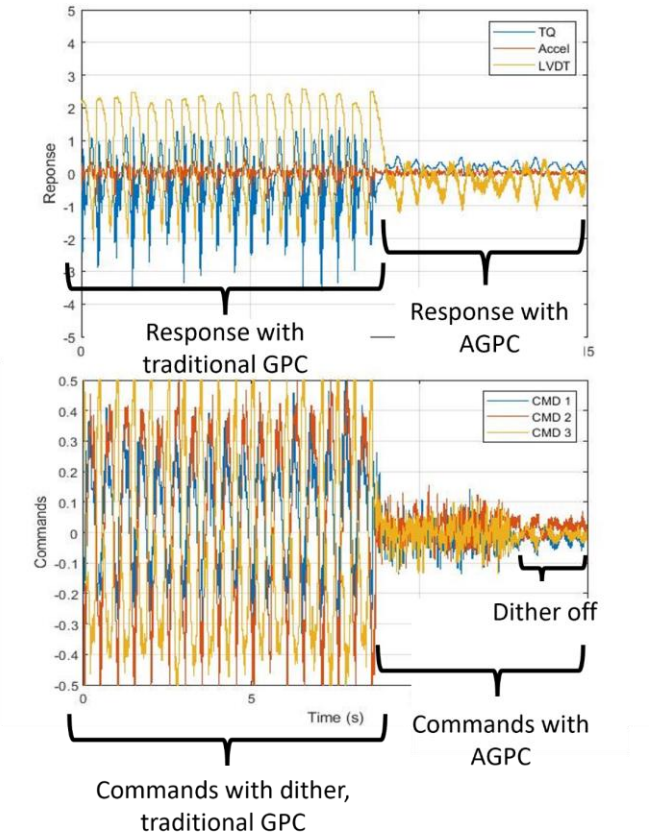

Figure 15. Closed-loop response of simple tiltrotor model with dither applied, traditional GPC and AGPC self-correcting algorithm, V=21.17 ft/s.

During experimental efforts, there were other instances where traditional GPC was able to stabilize the whirl-flutter instability of the simple tiltrotor model. However, most of these occurrences were earlier in the test effort prior to the installation of the LVDT and often resulted in static yaw divergence of the nacelle. Also, unfortunately, a setting error in the data system prevented the acquisition of time history data for these events. Variations in instrumentation were further explored in an effort to improve the response of the GPC and AGPC controllers. However, the small scale of the model and the limited quality of the RC model parts restricted the design options, and no variation was discovered that performed better than the example presented here. Consideration was given to further refining the simple tiltrotor model design, but the model had already served its purpose. GPC and AGPC were successfully implemented, and the results of the extensive analytical investigation and development were verified. Additionally, important lessons learned were revealed that vastly improved the safety of the experimental implementation of these control algorithms. Therefore, the research effort shifted focus to the TRAST model, which was precision machined, contains instrumentation of scientific quality, has reliable and repeatable actuators, is fully supported by research staff, has quality signal conditioners and data system components, and is ultimately the desired research platform that this research effort strives to impact.

Traditional GPC Applied to the TRAST Model

Applying an active control system to a complex rotorcraft model requires an incremental approach due to the risk to the model and facility. Dynamically-scaled rotor systems on flexible models with high-frequency hydraulics have the potential for catastrophic results should the controller fail, even on a hover test stand. Therefore, application of GPC and AGPC to the TRAST model was done first on the model with no blades and no rotation of the rotor system. The only control effector in this configuration was the mass of the swashplate and the resulting risk to model systems in this configuration was minimal. Once the controller and safety protocols proved satisfactory, the rotor system was rotated without the blades installed to verify that motor and drivetrain dynamics and associated electrical loads would not interfere with the controller. Finally, blades were added, and the model was run in the hover configuration with GPC and AGPC active.

Helicopter Mode with Inertial Shaker, Traditional GPC

The first test iterations were done in the helicopter mode with an inertial shaker using an internal vibrating mass operating in a sine sweep from 4.5 to 15 Hz over a period of 15 seconds. All three of the primary modes described earlier (wing out-of-plane bending, wing in-plane chord bending, and nacelle pitch) were excited by the shaker. Data records were acquired for a period of 15 seconds in order to capture the full sweep. Data records were manually triggered independent of the shaker commands and were started at times arbitrary to the period of the shaker sweep. The open-loop response of the TRAST model is shown Figure 16.

Initial attempts of applying GPC to the TRAST model involved using wing root bending, wing root chord, and nacelle pitch bending moment measurements and controls of collective, longitudinal, and lateral cyclic. However, in the helicopter mode at 90-degree nacelle angle using only the mass of the swashplate as an effector, cyclic controls are not capable of affecting wing chord or nacelle pitch modes. Therefore, the system ID characterized the response of signal noise to cyclic input rather than actual system behavior. As a result, the closed-loop response was violent and unstable. When individual actuator positions were used as the controls and the measured response was wing root out-of-plane bending, mid-span wing out-of-plane bending, and nacelle acceleration (aligned with the rotor shaft), then GPC performance was very effective. The lesson learned is that the selected control actuators must be able to effectively influence the measured response or GPC will not be effective.

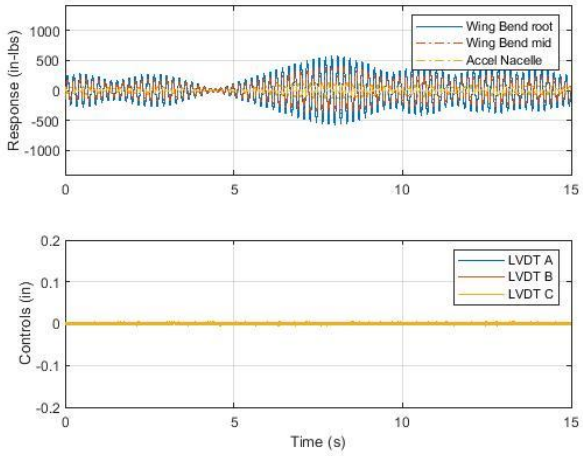

Figure 16. Open-loop response of TRAST, inertial shaker sweep, helicopter mode (90 deg), no blades.

An example of a system ID time history with orthogonal multisine excitation and the individual actuator positions as control input is shown in Figure 17. For the system ID, the inertial shaker was turned off since it created more vibration than the mass of the swashplate was able to excite.

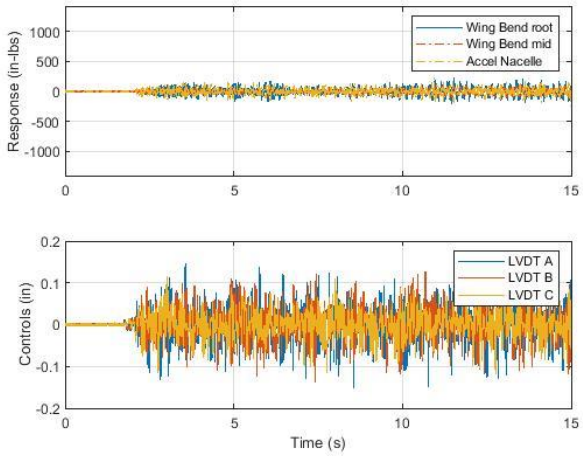

Figure 17. System ID of TRAST in helicopter mode, no blades.

Closed-loop time history data are shown in Figure 18 using this system ID. In this example, the system is initially open loop, and the controller is activated after the shaker excites the bending mode in resonance. As seen, the GPC controller is very effective at nearly eliminating the vibration from the inertial shaker. The increase in instrumentation quality and the ability of the actuators to influence the measured quantities has substantially improved the controller performance by comparison to the simple tiltrotor model. Additionally, by inspection of the LVDT command signals, one can see that the actuators are in unison inciting a collective response of the swashplate as one may expect.

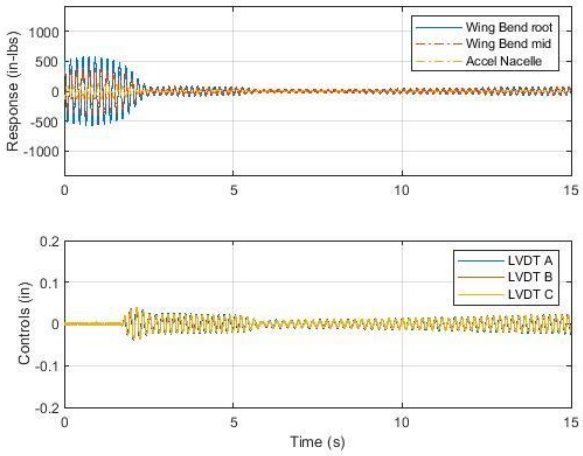

Figure 18. Open-loop then closed-loop response of TRAST in helicopter mode, traditional GPC with inertial shaker.

To experiment with the robustness of the controller, a series of 14-pound sandbags were added to the wing as shown in Figure 19 in order to alter the natural bending frequency of the model. The nominal wing out-of-plane bending frequency was approximately 5.5 Hz with the fairings removed as shown and was reduced to 5.0 Hz with three sandbags (42 pounds) in place. The frequency sweep used on the inertial shaker was reduced in bandwidth to better target the first bending mode and ran from approximately 4.5 to 6 Hz. Recall, the open-loop response with no sandbags was shown in Figure 16 and the response with three sandbags added is shown in Figure 20. The addition of the sandbags increased the inertia of the system and reduced the amplitude of the response. The closed-loop response of the system with sandbags using the same system ID acquired without sandbags is shown in Figure 21. The addition of the sandbags resulted in no degradation of the controller performance even though the natural frequency and mass of the system are different.

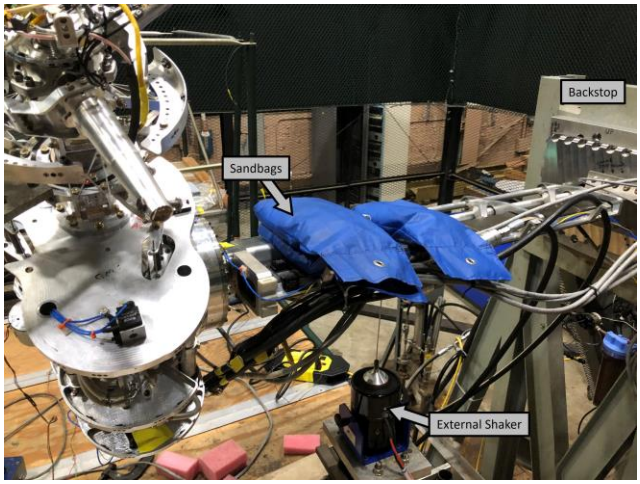

Figure 19. TRAST model with sandbags installed to alter the natural frequency of the wing.

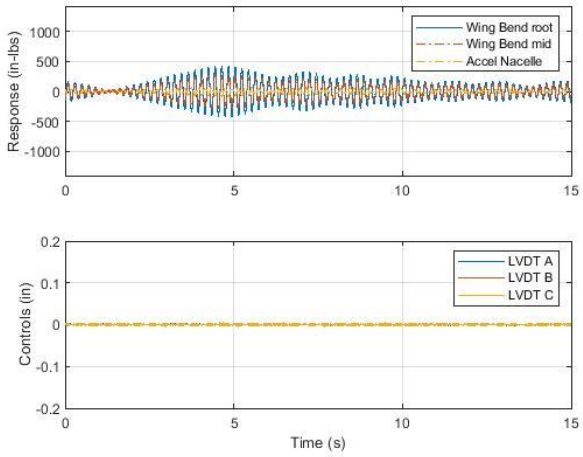

Figure 20. Open-loop response of TRAST, inertial shaker sweep with tighter bandwidth, three sandbags.

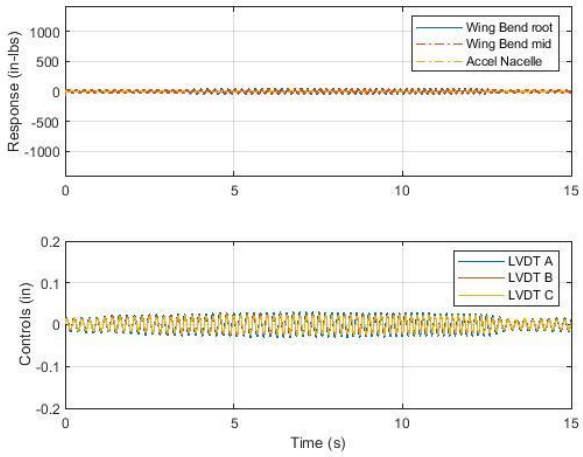

Figure 21. Closed-loop response of TRAST, inertial shaker sweep with tighter bandwidth, three sandbags.

60-deg Transition Mode with Inertial Shaker, Traditional GPC

Predominant aeroelastic modes of the TRAST model during wind-on testing typically involve out-of-plane wing bending, in-plane (chord) wing bending, and pylon pitch modes. However, the rotor-off testing thus far has been limited to control of the out-of-plane wing bending mode only due to the orientation of the nacelle and limited use of swashplate mass to suppress vibrations. In an effort to control additional modes of vibration, the nacelle was positioned in a transient position (transitioning between airplane and helicopter mode) at approximately 60 degrees to the horizontal so that swashplate motion could affect wing out-of-plane bending and chord modes. Additionally, two large irregular masses were added to the rotating frame of the swashplate in lieu of pitch-change (PC) link connections. These masses were placed 120-degrees apart where the PC links would be for two of the three blades and the rotor was rotated to a position such that the masses could influence pylon pitch and yaw motion. One mass was constructed from a thick aluminum plate and the other from steel. Each mass differed in geometry and were one pound and two pounds respectively in weight. These masses were placed to give more control authority in an off-axis directions using swashplate cyclic motion. A photo of the tilted nacelle and arbitrary masses is shown in Figure 22. In this image, the LVDT associated with one of the hydraulic actuators is more visible than previous images in addition to the swashplate and scissor assemblies being more visible.

Figure 22. TRAST model with nacelle at 60 degrees, arbitrary masses added to swashplate.

In this configuration, the inertial shaker was mounted to the pylon in the same orientation (relative to the pylon) as before such that the vibrating mass induces forces along the pylon axis parallel to the rotor shaft 60 degrees from the horizontal. The inertial shaker will therefore excite wing bending and

wing chord modes. However, its effect on pylon pitch is comparable to other nacelle orientations and does not excite the mode appreciably. Shown in Figure 23 is a time history of the open-loop shaker sweep from 4.5 to 15 Hz over a period of 15 seconds as done previously for the model in the helicopter mode. From this time history, one can note that the wing chord mode is now a dominant response in addition to the wing bending mode. Nacelle pitch is also excited slightly but is a very small response compared to the wing modes due to the orientation of the shaker.

System ID data were acquired using orthogonal multisine excitation in the same manner previously described for the model in the helicopter mode, but using wing out-of-plane bending, in-plane chord bending, and nacelle pitch strain gauges as response measurements. The closed-loop response using traditional GPC following the system ID is shown in Figure 24. In this response, the wing out-of-plane bending is almost entirely suppressed, but there is negligible impact on the wing chord mode. One should also note that the actuator response is no longer a symmetrical collective input, but rather an asymmetrical cyclic input. Finally, the data acquisitions for the open-loop and closed-loop responses were taken at arbitrary start times during continuous shaker sine sweep loops, so one should not try to temporally compare Figure 23 to Figure 24 as indicated by the different time periods of the resonant wing chord response.

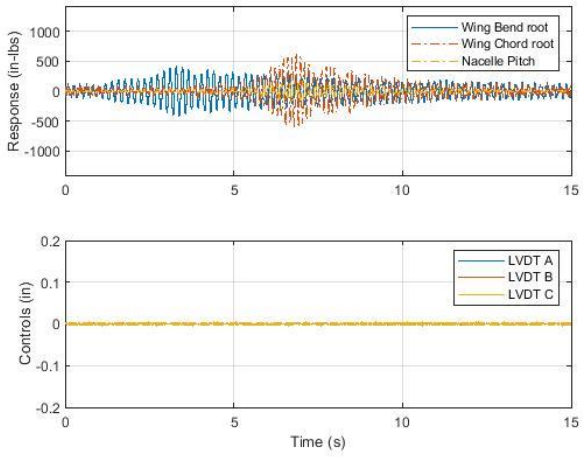

Figure 23. TRAST open-loop response, nacelle at 60 deg, inertial shaker.

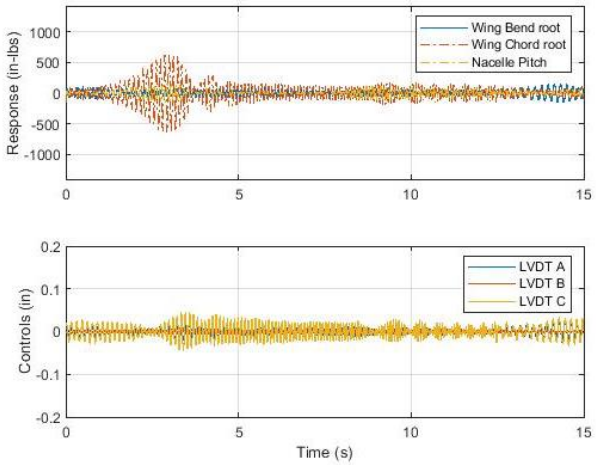

Figure 24. TRAST Closed-loop response, nacelle at 60 deg, inertial shaker.

60-deg Transition Mode, Simulated Instability, Traditional GPC

To simulate a dynamically unstable aeroelastic event, an external shaker was connected to the wing using a pushrod and was commanded using a control-feedback loop. This external shaker is visible in the image previously shown in Figure 19. The out-of-plane bending moment of the wing was measured and the shaker applied a force proportional to the derivative of the load (proportional to velocity) and in the direction of the displacement simulating a negative viscous damping. If left unaltered, the amplitude of the wing would grow exponentially until reaching a shaker limit. This creates an artificial "negative" damping or dynamic instability that mimics the behavior of flutter with an equivalent value of damping coefficient equal to 0.007.

GPC was then employed using the same mass of the swashplate and arbitrary masses as the control actuator. Time history data with the external shaker feedback loop is presented in Figure 25 for the TRAST model with the nacelle at 60 degrees. The first five seconds of the time history is open loop with the GPC controller inactive. During the open-loop portion, the exponential growth of the wing bending mode is apparent. If allowed to continue, load capability of the shaker would be exceeded, and the dynamic growth would be limited. However, at approximately five seconds, the GPC controller was activated, and swashplate actuation dampened the response of the wing. One can see that traditional GPC is very effective at stabilizing the instability. Consistent with past experiences, active controls are far more effective at stabilizing an instability than they are at reducing vibration and can do so with less control authority (Ref. 13).

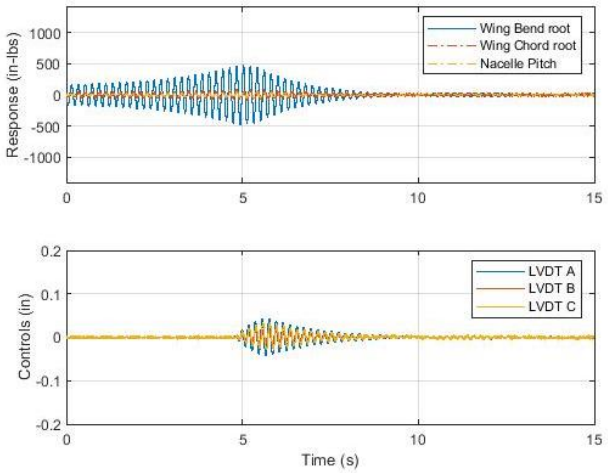

Figure 25. TRAST open- then closed-loop response, nacelle at 60 deg, external shaker to mimic instability, traditional GPC.

Rotor Operational Testing, Traditional GPC

Following the successful application of GPC to the TRAST model without the rotor installed and the development and application of various model safety protocols as described earlier and in Ref. 8, GPC was then applied to the model with the rotor installed and operational. Before blades were added, the arbitrary weights were removed from the swashplate and the PC links reattached to the blade pitch horns. Additionally, prior to blade installation, the controller was tested with the rotor hub spinning and no blades attached to verify that the electrical drive noise and pilot commands would not interfere with the GPC controller. The inertial shaker was then engaged and results similar to those presented earlier were acquired confirming the performance of the controller in the presence of the operating drivetrain.

For the TRAST model, the nominal rotor speeds are 909 rpm in hover and 727 rpm in airplane cruise mode as previously mentioned. During rotor runup, the out-of-plane bending mode of the wing is excited at 300 rpm and the wing chord bending mode is excited at 680 rpm. With a properly balanced rotor system, the model can dwell at these rotor speeds without danger to the model, but the vibrations are significant and serve as a great testbed for GPC vibration reduction. Also, the vibrations are significant enough that a system ID at these conditions is unlikely to be successful because of the signal to noise ratio.

System ID data were acquired at 270 rpm and 500 rpm thereby bracketing the out-of-plane bending resonance encountered at 300 rpm. The steady state open-loop response of the TRAST at 300 rpm in the helicopter mode is shown in Figure 26. Similarly, the closed-loop response of the model with system ID data acquired at 500 rpm and 270 rpm are shown in Figure 27 and Figure 28 respectively. For both of these data records, the time history begins open loop, and the loop is closed after approximately two seconds.

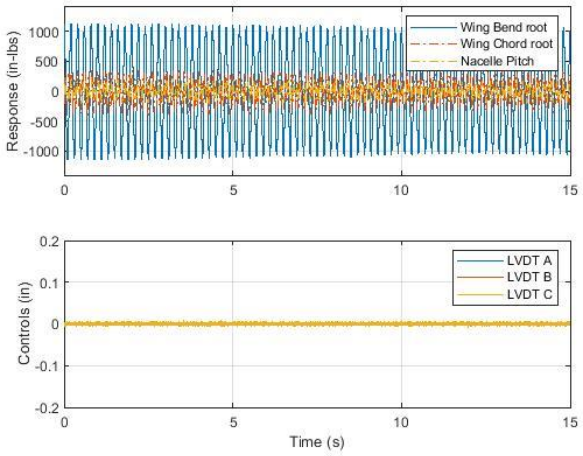

Figure 26. TRAST open-loop response, helicopter mode with blades on at 300 rpm, resonant response.

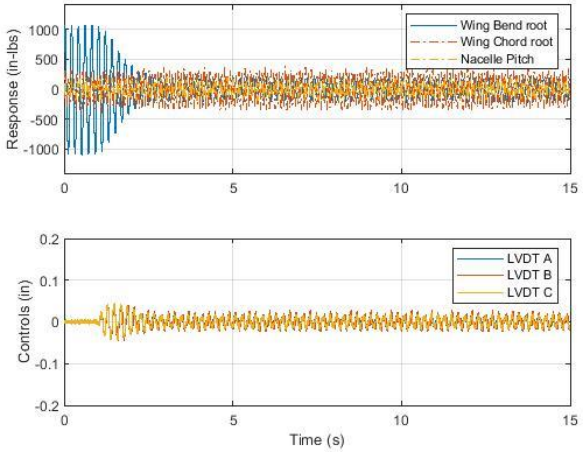

Figure 27. TRAST closed-loop response, helicopter mode blades on at 300 rpm, system ID acquired at 500 rpm.

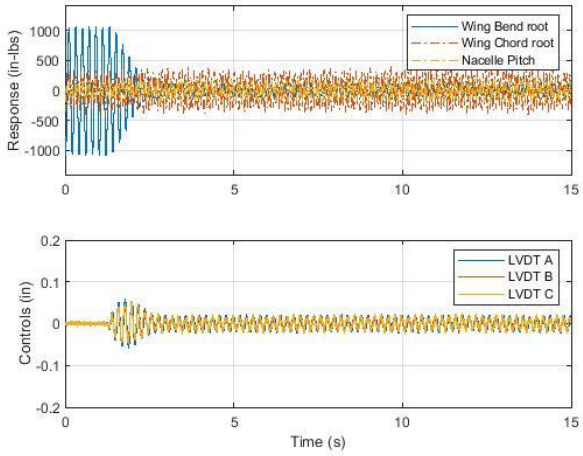

Figure 28. TRAST closed-loop response, helicopter mode blades on at 300 rpm, system ID acquired at 270 rpm.

Both system IDs from 270 or 500 rpm are very effective at suppressing the wing bending response and exhibit similar steady state vibration. However, the controller using the system ID acquired at 270 rpm suppresses the bending mode noticeably faster than the controller using the system ID acquired at 500 rpm. This is likely because the behavior of the model at 270 rpm is more representative of the behavior at 300 rpm than 500 rpm. Traditional GPC was also tested at various other rotor speed conditions with and without the inertial shaker yielding similar results to those presented without the rotor.

Advanced GPC Applied to the TRAST Model

There are some conditions in the previous traditional GPC examples that lend themselves well to testing the performance improvement potential of AGPC. The first case is the inertial shaker with the nacelle at 60 degrees and arbitrary masses installed on the swashplate. The result of AGPC compared to the previously presented traditional GPC performance for the model in this configuration is shown in Figure 29. AGPC significantly improved the wing chord response at the expense of the wing out-of-plane bending response. The peak wing bending is increased from 152 to 289 in-lbs, a factor of 1.9, and the peak chord response is reduced from 640 to 359 in-lbs, a factor of 1.8. Although difficult to observe in Figure 29, nacelle pitch is also reduced from 192 to 92 in-lbs, a factor of 1.8. Therefore, it is difficult to determine which system results in better overall vibration reduction. However, it is interesting to note that AGPC successfully suppresses multiple modes whereas traditional GPC could only suppress the wing out-of-plane bending mode, even when the system ID is acquired at the same condition. Additionally, AGPC realizes a notable reduction in actuator workload over most of the time history.

Another comparison of traditional GPC and AGPC was conducted with the simulated dynamic instability. In this application, dither was added while the system was closed loop in order to improve the figures of merit. The resulting difference in performance is apparent by inspection of Figure 30 which shows a noticeable increase in system damping using AGPC.

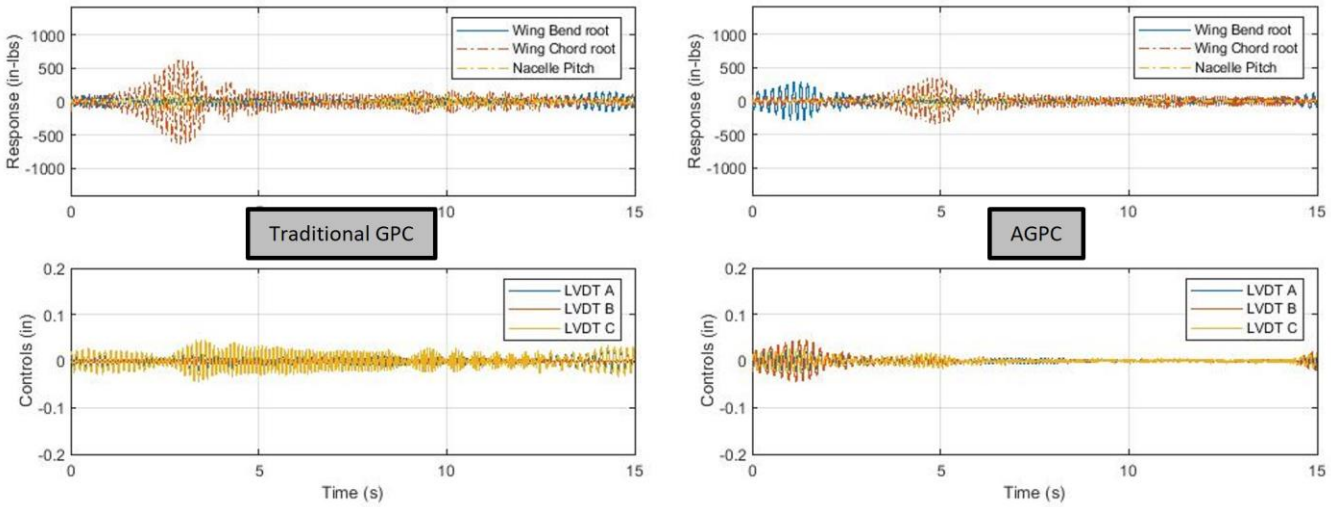

Figure 29. TRAST closed-loop response with inertial shaker, comparison between traditional GPC and AGPC.

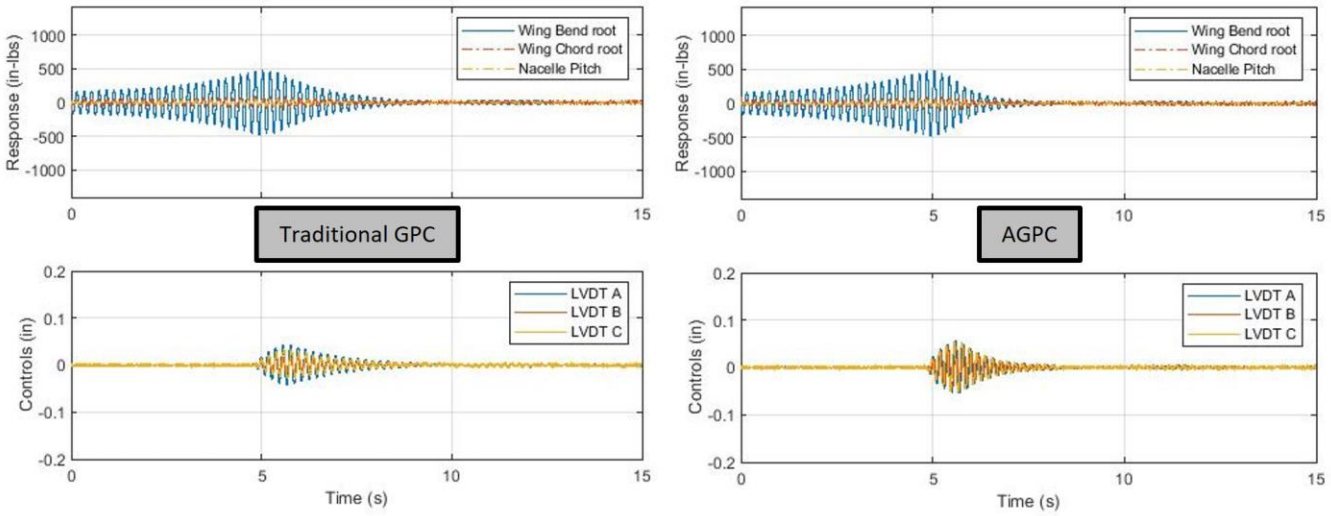

Figure 30. TRAST open then closed-loop response, nacelle at 60-dg transition, external shaker to mimic instability.

The ability of AGPC to perform better than traditional GPC at the same conditions where the system ID was acquired is not the intent of AGPC development and this result was surprising. Rather, the intent is to develop the ability of AGPC to improve controller performance when the system is operating at conditions removed from one in which the system ID was acquired, and traditional GPC breaks down such as that demonstrated with the simple tiltrotor model. Therefore, AGPC was also evaluated with the TRAST model during rotor-on operation to evaluate the ability of AGPC to improve controller performance at resonant conditions.

The resonant condition at 300 rpm offers an opportunity to test the adaptability of AGPC as intended since the acquisition of a system ID at this resonant condition using traditional methods is difficult due to the poor signal to noise ratios. Albeit traditional GPC control still works very well at 300 rpm with system ID data acquired at nearby conditions. The results of AGPC and a direct comparison to the performance of traditional GPC with the system ID acquired at 270 rpm is shown in Figure 31. As seen, AGPC is able to suppress the bending mode noticeably faster and also reduces the steady state vibrations of the wing chord and nacelle pitch modes by a slight amount. Since the resonant mode is the out-of-plane wing bending mode, one can see the steady state response better if the wing chord and nacelle pitch signals are removed. The same data record is shown in Figure 32 with only the out-of-plane bending mode represented in the response traces. As seen, AGPC successfully outperformed traditional GPC at suppressing the wing bending mode at the resonant rpm.

AGPC was also employed at the 680 rpm hover condition that excites wing chord in resonance. Similar to the wing out-of-plane bending mode, the model can tolerate dwelling at 680 rpm, but the response is large and traditional GPC cannot acquire a system ID at this condition. An open-loop system ID was acquired at the nearby cruise rotor speed of 727 rpm. The response of the system at 680 rpm with traditional GPC using the system ID acquired at 727 rpm is shown in Figure 33. As shown, GPC is very effective at reducing the resonant wing chord vibration and nacelle pitch.

Similarly, AGPC was employed at 680 rpm and a comparison of the controller performance to traditional GPC using the system ID acquired at 727 rpm is also shown in Figure 33. As observed, AGPC is more effective than traditional GPC at reducing the resonant wing chord vibration. For clarity, Figure 34 contains the same time histories with the wing chord and actuator B traces removed for clarity. In this figure, the ability of the controllers to suppress nacelle pitch and out-of-plane bending is more apparent. AGPC is also more capable of suppressing nacelle pitch than traditional GPC by a significant amount. However, the wing out-of-plane bending vibration is slightly increased with AGPC, but with comparable peak values to those observed with traditional GPC due to additional low-frequency content. Since this mode has by far the least amount of response at this condition, this slight increase is considered negligible compared to the overall vibration reduction of the system.

These experimental results with the TRAST model lend confidence to the ability of AGPC to stabilize the TRAST model farther beyond the flutter stability boundary than possible with traditional GPC efforts, similar to what was demonstrated with the simple tiltrotor model. Future research will investigate the use of AGPC compared to traditional GPC in wind-tunnel testing of TRAST in an effort to demonstrate improved stability augmentation and vibration reduction of tiltrotor aircraft than other state-of-the-art options and with less user workload or system excitation.

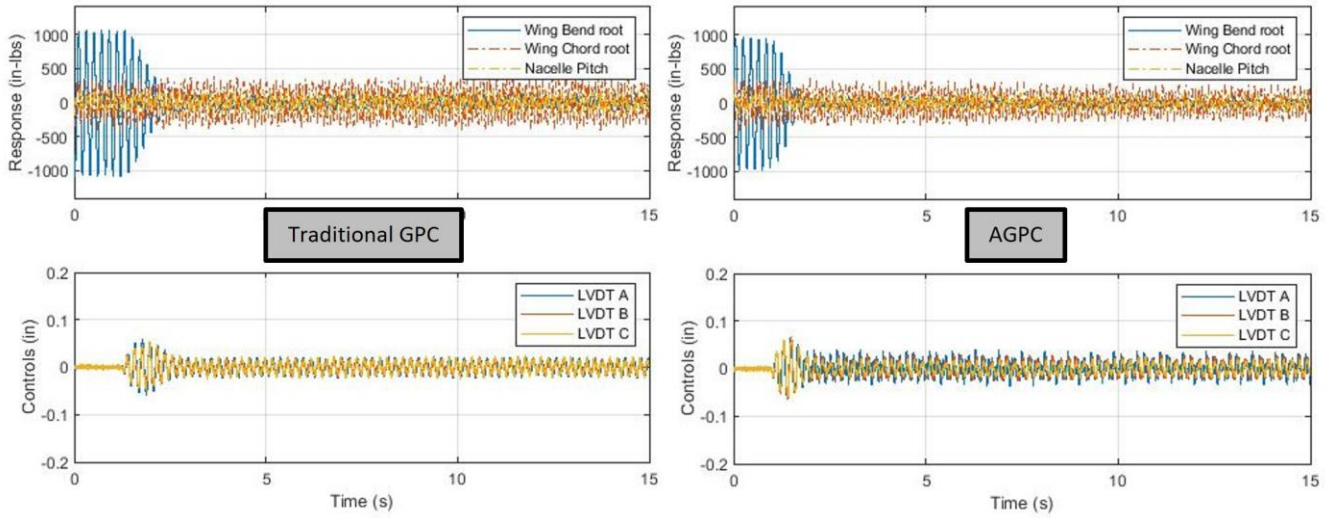

Figure 31. TRAST Closed-Loop Response, Helicopter Mode with Blades On at 300 rpm Comparison of 270 rpm System ID and AGPC.

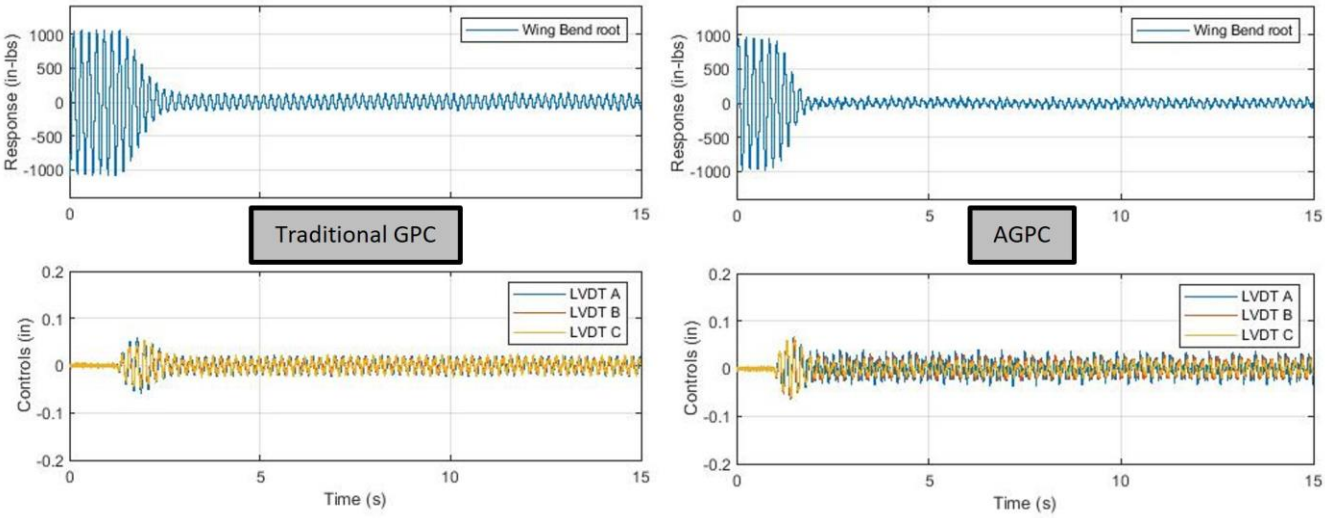

Figure 32. TRAST Closed-Loop Response, Helicopter Mode with Blades On at 300 rpm, Comparison of 270 rpm System ID and AGPC, Bending Response Only

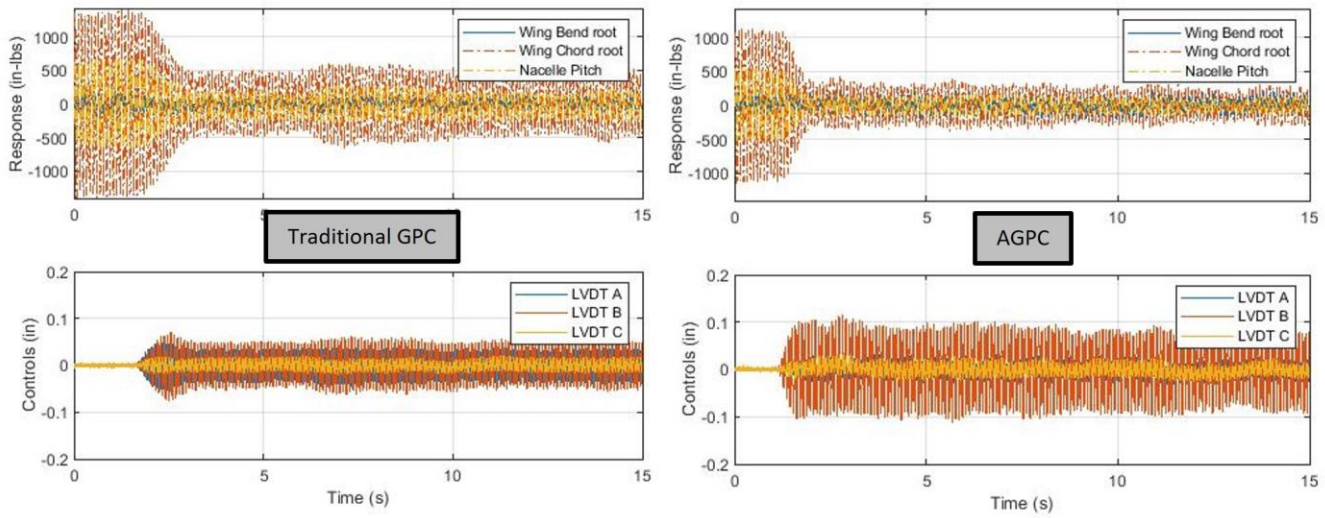

Figure 33. TRAST Closed-Loop Response, Helicopter Mode with Blades On at 680 rpm, Comparison of 727 rpm System ID and AGPC.

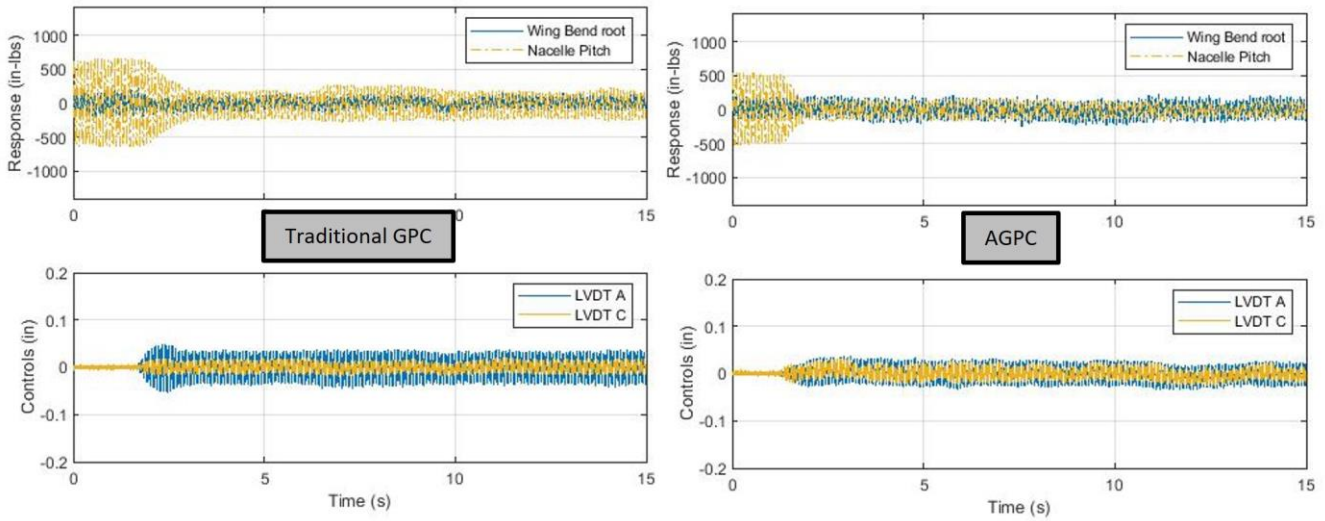

Figure 34. TRAST Closed-Loop Response, Helicopter Mode with Blades On at 680 rpm, Comparison of 727 rpm System ID and AGPC, Wing Bending and Nacelle Pitch Response Only, No Actuator B.

For all of the experimental results presented in this paper, the same controller was used without any significant modification. Additionally, the same modeling parameters of sample rate, sample size, order of the model, and horizon sizes were used. This is a testament to the utility of GPC and AGPC, in that the same control law can stabilize multiple models as vastly different as the simple tiltrotor model and TRAST in multiple different configurations. The same controller is effective even with and without rotor blades installed by using experimental data to determine system behavior. This same controller and selection of modeling parameters was successful across these different models because the primary dynamics of interest were of similar frequency. Furthermore, if the measurement instrumentation is gained such that approximately the same voltage values correspond to maximum allowable responses and if approximately the same voltage command values correspond to maximum allowable excitation, then no change to the weighting matrices is required for the controller to be functional across these different systems. However, adjustment of the weighting matrices would be recommended to optimize the controller for a particular model or configuration (Ref. 8). Finally, with the same selection of modeling parameters, approximately the same figures of

merit values indicate acceptable controller performance and system IDs for purposes of AGPC implementation.

CONCLUSIONS

The complex nature of tiltrotor dynamic control does not lend itself well to conventional control theory as the equations of motion become prohibitively complex and nonlinear by comparison to fixed-wing aircraft or many other dynamic systems. This research effort has therefore focused upon the use of predictive and adaptive control methodologies using ARX models. These models leverage experimental acquisition of input/output behavior to derive a system identification of a multiple-input multiple-output system. GPC is an advanced form of the ARX model that shares similarities to conventional optimal control theory and has been shown to outperform many other control options. Although it is a very effective controller, traditional GPC effectiveness and stability can erode as flight conditions change from those used to experimentally derive the system ID and some conditions prohibit the use of traditional GPC due to dynamic instabilities that cannot be suppressed enough to acquire reliable system ID data. AGPC is an attempt to overcome these challenges and can improve controller performance. Self-adaptive AGPC was developed, introduced, and demonstrated analytically in previous work and experimentally in the current work. It was shown to be very useful and effective at self-adjustment, and it consistently outperformed traditional GPC at conditions removed from those where the system ID was acquired. Also, unexpectedly, it outperformed traditional GPC in some cases when used at the same conditions that the system ID was acquired. Furthermore, AGPC can make adjustments with negligible impact to system response by contrast to traditional GPC that requires significant excitation of the system.

Adapting a poor performing control algorithm while not interfering with a good performing controller is the intent of AGPC. Therefore, figures of merit were developed and introduced in the present work to quantify the effectiveness of a working controller and to quantify the likelihood that individual input/output signals are distinguishable enough to properly characterize the system. When these figures of merit are satisfied, the self-adaptive AGPC controller methodology consistently improved controller performance and was shown to stabilize a dynamic system that traditional GPC could not.

Author contact:
Thomas G. Ivanco, thomas.g.ivanco@nasa.gov
Andrew R. Kreshock, andrew.r.kreshock@nasa.gov
Robert P. Thornburgh, robert.p.thornburgh@nasa.gov
Matthew L. Wilbur, matt.wilbur@cox.net
Brett A. Newman, bnewman@odu.edu

REFERENCES

1 Kreshock, A. R., Thornburgh, R. P., and Wilbur, M. L., "Overview of the TiltRotor Aeroelastic Stability Testbed," presented at the AIAA SciTech Forum, San Diego, CA, Jan. 2022, AIAA 2022-0566. doi: 10.2514/6.2022-0566.

2 Ivanco, T. G., "Unique Testing Capabilities of the NASA Langley Transonic Dynamics Tunnel, an Exercise in Aeroelastic Scaling," presented at the AIAA SciTech Forum, San Diego, CA, Jun. 2013. AIAA 2013-2625. doi: 10.2514/6.2013-2625.

3 Clarke, D. W., Mohtadi, C., and Tuffs, P. S., "Generalized Predictive Control - Part I. The Basic Algorithm," *IFAC*, vol. 23, no. 2, pp. 137–148, 1987.

4 Juang, J and Phan, M, "Deadbeat Predictive Controllers," NASA Langley Research Center, NASA TM 112862, May 1997. Available: https://ntrs.nasa.gov/archive/nasa/casi.ntrs.nasa.gov/19970027551.pdf

5 Kvaternik, R. G., Juang, J., and Bennett, R. L., "Exploratory Studies in Generalized Predictive Control for Active Aeroelastic Control of Tiltrotor Aircraft," NASA Langley Research Center, Hampton, VA, NASA TM 2000-210552, 2000.

6 Ivanco, T. G., Kang, H., Kreshock, A. R., Thornburgh, R. P., and Newman, B. A., "Generalized Predictive Control for Active Stability Augmentation and Vibration Reduction on an Aeroelastic Tiltrotor Model," presented at the AIAA SciTech Forum, San Diego, CA, Jan. 2022, AIAA 2022-0570. doi: 10.2514/6.2022-0570.

7 Kvaternik, R. G., "Generalized Predictive Control of Dynamic Systems with Rigid-Body Modes," NASA, Langley Research Center, Hampton, VA, Technical Memo NASA TM-2013-217976, Apr. 2013.

8 Ivanco, T. G., Newman, B. A., Alberts, T. E., Bawab, S. Y., Baysal, O., and Silva, W. A., "Advanced Generalized Predictive Control and its Application to Tiltrotor Aircraft for Stability Augmentation and Vibration Reduction," Ph.D. Dissertation, Old Dominion University, Norfolk, VA, 2022. doi: 10.25777/qbqq-ez94

9 Kvaternik, R. G. *et al.*, "An Experimental Evaluation of Generalized Predictive Control for Tiltrotor Aeroelastic Stability Augmentation in Airplane Mode of Flight," NASA Langley Technical Report Server, Technical Report 20010059025, Jan. 2001. Presented at the American Helicopter Society International Forum, Washington D.C., May 9-11, 2001.

10 Klein, V. and Morelli, E. A., *Aircraft System Identification, Theory and Practice*. in AIAA Education Series. Reston, VA: American Institute of Aeronautics and Astronautics, Inc., 2006.

11 Simmons, B. M. and Murphy, P. C., "Aero-Propulsive Modeling for Tilt-Wing, Distributed Propulsion Aircraft Using Wind Tunnel Data," *Journal of Aircraft*, vol. Vol. 59, No. 5, pp. 1162–1178, Oct. 2022, doi: 10.2514/1.C036351.

12 Simmons, B. M., "Evaluation of Response Surface Experiment Designs for Distributed Propulsion Aircraft Aero-Propulsive Modeling," presented at the AIAA SciTech conference, Jan. 2023, AIAA 2023-2251. doi: 10.2514/6.2023-2251

13 Simmons, B. M., "Efficient Variable-Pitch Propeller Aerodynamic Model Development for Vectored-Thrust eVTOL Aircraft," presented at the AIAA Aviation Conference, Chicago, IL, Jun. 2022, AIAA 2022-3817. doi: 10.2514/6.2022-3817